

***Ab initio* calculations of excitons in GaN**Robert Laskowski,<sup>1</sup> Niels Egede Christensen,<sup>1</sup> Gilles Santi,<sup>1</sup> and Claudia Ambrosch-Draxl<sup>2</sup><sup>1</sup>*Department of Physics and Astronomy, University of Århus, DK-8000 Århus C, Denmark*<sup>2</sup>*Institute of Physics, University of Graz, Universitätsplatz 5, A-8010 Graz, Austria*

(Received 4 February 2005; revised manuscript received 13 April 2005; published 7 July 2005)

The optical absorption and excitonic properties of wurtzite GaN are investigated by means of an *ab initio* approach taking into account electron-hole correlations. This is done by solving the Bethe-Salpeter equation, using the results of density functional theory calculations as a starting point. Our main focus is the calculation of the binding energies of bound excitons, as well as their dependence on structural parameters and details of the electronic structure.

DOI: [10.1103/PhysRevB.72.035204](https://doi.org/10.1103/PhysRevB.72.035204)

PACS number(s): 71.15.Qe, 71.35.Cc, 78.20.Ci, 78.40.Fy

**I. INTRODUCTION**

GaN is a tetrahedrally coordinated semiconductor characterized by high ionicity, short bonds, low compressibility, high thermal conductivity, and large band gap ( $E_g > 3$  eV). These properties make it of great technological importance especially for optoelectronic applications in the blue/UV range of the spectrum, such as blue-light emitting diodes, blue-UV lasers, solar blind photodetectors, or high-temperature, high-field heterojunction bipolar devices.<sup>1-4</sup> GaN crystallizes in two phases: the wurtzite structure (hexagonal, 2H) with space group  $C_{6v}^4$ , and the zinc blende one (cubic, 3C) with space group  $T_d^2$ , which is less common (difficult to grow) and not so extensively studied experimentally. Here we will consider only the most stable wurtzite phase. The primitive cell contains four atoms. The equilibrium structural parameters are  $a=6.0282$  a.u.,  $c=9.8057$  a.u., and the Ga-N nearest neighbor distance in the  $c$  direction,  $u=0.377$  (in units of the  $c$  axis length).

The optical properties of GaN have been studied by several authors from both theoretical and experimental points of view. Theoretical *ab initio* calculations within the density functional theory (DFT) have been reasonably successful within well-known limitations. For example, a study of the pressure dependence of the band gap ( $E_g$ ) and the refractive index obtained a satisfactory agreement between experiment and theory and showed that GaN is a direct gap semiconductor.<sup>5</sup> In addition, DFT calculations of the optical and structural properties of GaN and other nitrides under pressure were compared to experiments in Ref. 6. *Ab initio* calculations of dielectric and phonon properties were also reported.<sup>7</sup> Despite the relative success of the first-principles calculations it is clear that these standard approaches are unable to reproduce properly all details of the optical properties known from experiment since they do not include electron-hole ( $e-h$ ) interactions. Comparison between the measured and calculated spectra shows that the theory tends to underestimate the imaginary part of the dielectric function  $\epsilon_2(\omega)$  in the low energy ( $\hbar\omega$ ) regime and overestimate it for high photon energies. Moreover, the bound excitons are not described at all. The first calculation of the dielectric function in GaN including electron-hole interactions was reported by Benedict and Shirley<sup>8</sup> and Benedict *et al.*<sup>9</sup> and these theoret-

ical results represented a significant improvement over those based on the independent particle approach. Their computational scheme<sup>10-12</sup> characterizes the  $e-h$  interaction with the effective two-body Hamiltonian emerging from the many-body perturbation theory expressed in terms of the so-called Bethe-Salpeter equation (BSE).<sup>13-18</sup> This approach has already been successfully used to study both inorganic<sup>8,12,19</sup> as well as organic<sup>20,21</sup> semiconductors.

Owing to the particular importance of the excitons in GaN to optical properties, they have become interesting to the experimental community and the binding energies of the three lowest excitonic states have been determined by a number of experimental techniques.<sup>22-28</sup> The results all lie in the range 18–28 meV. This relatively broad spread has probably two reasons. First, some of the measurements are done on epitaxial layers with large induced strain, which can affect the measured binding energies. Second, the analysis is generally based on fitting the peak positions in the absorption spectrum to Elliott's theory<sup>29</sup> (hydrogen-like spectrum), meaning that any mislabeling of the peaks would lead to incorrect binding energies.

The aim of this work is to calculate the binding energies of bound excitons as well as the absorption spectra in wurtzite GaN within the BSE approach. As a small variation of the geometry of the unit cell can strongly affect electric field gradients (which are very sensitive to the details of the local charge distribution),<sup>30</sup> we will investigate the sensitivity of the binding energies to structural parameters. Furthermore, our DFT calculations being performed within the generalized gradient approximation (GGA) to exchange-correlation, we will also examine the influence of that approximation on the excitonic properties by varying details of the band structure (i.e., band gap and band mass). Finally, our absorption spectra for this material will be compared to available experiments as well as to previous calculations.<sup>8</sup>

The paper is organized as follows. The next section describes the basic ingredients of the computational methods we use. Section III presents and discusses the results of our calculations. Finally, Sec. IV concludes and summarizes our findings.

**II. THEORY AND METHOD**

The computational scheme for calculating the optical response that takes into account electron-hole interaction em-

ployed in this work has already been worked out by several authors.<sup>10–12</sup> The rigorous theoretical description of the  $e$ - $h$  excitations is based on solving the equation of motion of the two-particle Green's function, known as the Bethe-Salpeter equation (BSE). This equation of motion can be approximated by an effective eigenvalue problem with the so-called BSE Hamiltonian.<sup>17,18</sup> The practical approach generally consists of two steps. In the first one, the single particle valence and conduction quasiparticle states have to be calculated. This is often done by correcting the DFT eigenstates with the  $GW$  approximation<sup>12,31,32</sup> (where  $G$  and  $W$  are the Green's function and the screened Coulomb potential, respectively). In the second one, the eigenvalue equation

$$\sum_{v'c'k'} H_{vc\mathbf{k},v'c'\mathbf{k}'}^e A_{v'c'\mathbf{k}'}^\lambda = E^\lambda A_{vc\mathbf{k}}^\lambda, \quad (1)$$

is formulated in the basis of electron and hole quasiparticle states. The excitation spectrum is given by the eigenvalues of this equation. In this formalism only the direct transitions leading to  $e$ - $h$  excited states with infinite lifetime are considered. In Eq. (1),  $H^e$  is the effective  $e$ - $h$  interaction,  $vc\mathbf{k}$  denotes an elementary excitation taking place at a point  $\mathbf{k}$  of the Brillouin zone (BZ), from a valence ( $v$ ) to a conduction ( $c$ ) band. The actual excitonic eigenstate is a linear combination of such elementary excitations. In GaN, the spin-orbit coupling (SOC) is found to have only minor effects on the bands' energies and is therefore neglected in the BSE calculations, thereby considerably simplifying the numerical computations. The effective BSE Hamiltonian is thus a sum of three terms

$$H^e = H^{\text{diag}} + H^{\text{dir}} + 2\eta H^x, \quad (2)$$

which are defined as

$$H_{vc\mathbf{k},v'c'\mathbf{k}'}^{\text{diag}} = (\varepsilon_{v\mathbf{k}} - \varepsilon_{c\mathbf{k}'} + \Delta) \delta_{vv'} \delta_{cc'} \delta_{\mathbf{k}\mathbf{k}'}, \quad (3)$$

$$H_{vc\mathbf{k},v'c'\mathbf{k}'}^{\text{dir}} = - \int d^3r d^3r' \psi_{v\mathbf{k}}(\mathbf{r}) \psi_{c\mathbf{k}'}^*(\mathbf{r}') \times W(\mathbf{r}, \mathbf{r}') \psi_{v'\mathbf{k}'}^*(\mathbf{r}) \psi_{c'\mathbf{k}'}(\mathbf{r}'), \quad (4)$$

$$H_{vc\mathbf{k},v'c'\mathbf{k}'}^x = \int d^3r d^3r' \psi_{v\mathbf{k}}(\mathbf{r}) \psi_{c\mathbf{k}'}^*(\mathbf{r}) \times \bar{v}(\mathbf{r}, \mathbf{r}') \psi_{v'\mathbf{k}'}^*(\mathbf{r}') \psi_{c'\mathbf{k}'}(\mathbf{r}'). \quad (5)$$

The parameter  $\eta$  in front of the exchange term  $H^x$  distinguishes singlet ( $\eta=1$ ) from triplet excitations ( $\eta=0$ ). In this work we concentrate on the singlet excitations. The direct interaction term  $H^{\text{dir}}$  describes the screened Coulomb attraction ( $W$ ) between the hole and the electron. The necessary dielectric matrix is calculated within the random phase approximation (RPA) including local field effects.<sup>33,34</sup> Note that the exchange part of the Hamiltonian involves the short-range part of the bare Coulomb interaction ( $\bar{v}$ ). Neglecting the direct and exchange terms leaves only the diagonal part of the Hamiltonian ( $H^{\text{diag}}$ ) and results in the independent  $e$ - $h$  approximation. The quasiparticle states, which are the basis of the BSE Hamiltonian, are often well approximated

by the DFT wave functions<sup>32</sup> in contrast to the conduction band quasiparticle energies which are not. Thus, in order to simplify calculations, we construct our Hamiltonian directly using the DFT eigenstates and we approximate the self-energy by an appropriate rigid shift of the conduction bands. This so-called “scissors operator” or “scissors shift”  $\Delta$  is determined by adjusting the DFT band gap to the measured one.<sup>28</sup> As this shift only appears explicitly in the diagonal part of the Hamiltonian, it has no direct effect on the binding energies. It influences however the excitonic eigenenergies indirectly through its effect on the screening interaction (the scissor shifted DFT states are used when calculating the screening within the RPA).

The linearized augmented plane wave method plus local orbitals (LAPW+LO) is used to calculate single particle states.<sup>35</sup> We have used the improved form of the basis set, where the linearization is moved from augmented plane waves into additional local orbitals.<sup>36</sup> The implementation of the BSE scheme within the LAPW method has already been applied to centrosymmetric systems<sup>21,37</sup> and described in detail in Ref. 38. In order to study GaN, we extended this original implementation to structures without inversion symmetry. Finally, all DFT calculations were performed within GGA, using the Perdew, Burke, and Ernzerhof parametrization of the exchange-correlation potential.<sup>39</sup>

Calculating excitation energies involves diagonalizing the eigenvalue equation, Eq. (1). It turns out that numerical convergence requires an enormously dense  $\mathbf{k}$ -point sampling. However, only excitations between the topmost valence and the lowest conduction bands and highly localized (in  $\mathbf{k}$  space) around the center of the BZ ( $\Gamma$  point) enter into the excitonic wave function of the lowest bound excitons. This means that the BSE Hamiltonian is block diagonal in the  $\mathbf{k}$  index around  $\Gamma$  and that the outer region does not need to be sampled at all. The number of  $\mathbf{k}$  points can thus be lowered down to a level making the direct diagonalization of Eq. (1) possible. A similar approach has been used for calculation of the binding energies of excitons in GaAs.<sup>12</sup> We noticed that, when using a too coarse sampling, the excitonic states are composed solely of excitations at the  $\Gamma$  point ( $\mathbf{k}=0$ ),  $A_{vc\mathbf{k}}^\lambda$  being zero everywhere else, making them fully delocalized in real space. Evaluating the  $\mathbf{k}=\mathbf{k}'=0$  element of the direct interaction matrix,  $H_{vc\mathbf{k},v'c'\mathbf{k}'}^{\text{dir}}$ , necessitates, however, the use of the limit of an analytical approximation [see Eq. (18) in Ref. 38]. This approximation has no consequence for the calculated excitation energies if sufficiently many other  $\mathbf{k} \neq 0$  points carry a significant part of the total exciton wave function, but it completely determines them in the fully delocalized case (in real space). This leads to an erroneous estimate if this full delocalization is an artefact of a poor  $\mathbf{k}$ -point sampling. A proper sampling should therefore be sufficiently dense to describe the variation of the excitonic wave function (i.e.,  $A_{vc\mathbf{k}}^\lambda$ ) in  $\mathbf{k}$  space and thus its localization in real space. Two parameters control the sampling density, i.e., the volume of the sampled region and the number of  $\mathbf{k}$  points inside. We have found that, for the experimental structure parameters ( $c/a$ ,  $u$ , and volume), accurate results for ground as well as higher lying bound states are obtained by sampling a  $1/12 \times 1/12 \times 1/8$  fraction of the BZ with a  $11 \times 11 \times 11$

mesh (corresponding to nearly 2 million points in full BZ). However, well converged results for the excitonic ground states only and for volume changes of up to  $\pm 4\%$  can already be reached by sampling a  $1/9 \times 1/9 \times 1/6$  part of the BZ with a  $9 \times 9 \times 9$  mesh (equivalent to using nearly half a million  $\mathbf{k}$  points in full BZ). Note that only points that are consistent with the hexagonal symmetry are kept. It must be added that, for larger compressions (smaller unit cell volumes), the size of the sampled region had to be further decreased.

Calculating the imaginary part of the dielectric function ( $p_i$  being the momentum operator projected onto the polarization direction of the electrical field)

$$\varepsilon_2(\omega) = \frac{8\pi^2}{\Omega} \sum_{\lambda} \left| \sum_{vck} A_{vck}^{\lambda} \frac{\langle v\mathbf{k}|p_i|c\mathbf{k}\rangle}{\varepsilon_{ck} - \varepsilon_{vk}} \right|^2 \times \delta(E^{\lambda} - \omega), \quad (6)$$

requires a complete sampling of the full BZ. Fortunately, a much lower sampling density can be used in this case, as we are not interested in the very fine details of the absorption edge but only in the overall shape of  $\varepsilon_2(\omega)$ . A much broader region of excitation energies needs, however, to be considered in order to cover a wide range of photon energies, meaning that more conduction and valence bands have to be included in the BSE Hamiltonian. For example, for the  $15 \times 15 \times 10$   $\mathbf{k}$ -point mesh that gives converged results, with six valence and eight conduction bands, the size of the Hamiltonian is as large as 108 000. Diagonalizing such a large matrix would be impractical and we use the so-called “time evolution” algorithm introduced by Schmidt *et al.*<sup>40</sup> where  $\varepsilon_2(\omega)$  can be evaluated without explicitly calculating excitonic eigenvalues and eigenvectors.

### III. RESULTS AND DISCUSSION

#### A. Dielectric function

Before presenting and discussing in detail our calculated excitonic spectra and wave functions, we show the calculated absorption spectrum (i.e., the imaginary part of the dielectric function) and compare it to previous calculations.<sup>8</sup> The calculated  $\varepsilon_2(\omega)$  is shown in Fig. 1. As expected, the band gap calculated by the GGA underestimates the experimental value of 3.45 eV (Ref. 28) and an *ad hoc* scissors shift of about 1.4 eV was applied in order to correct the position of the conduction bands. Note that this scissors shift is applied to both DFT and BSE results presented in Fig. 1. Our absorption spectra are very similar to those published previously (both in terms of the positions of the peaks and their relative intensities), despite the differences in the treatment of the screened Coulomb interaction. The main differences appear for the case of perpendicularly polarized light where the peak intensities in their spectrum decrease with increasing photon energy compared to our spectrum. This discrepancy can, in fact, be traced back to the differences at the one-particle calculation level. Additionally, Fig. 1 shows that the effect of including the *e-h* interactions (BSE), apart from shifting down the DFT spectra, seems mainly to enhance  $\varepsilon_2(\omega)$  in the low energy region (up to about 6 eV) and reduce it somewhat at the end of the spectra (from about 12 eV).

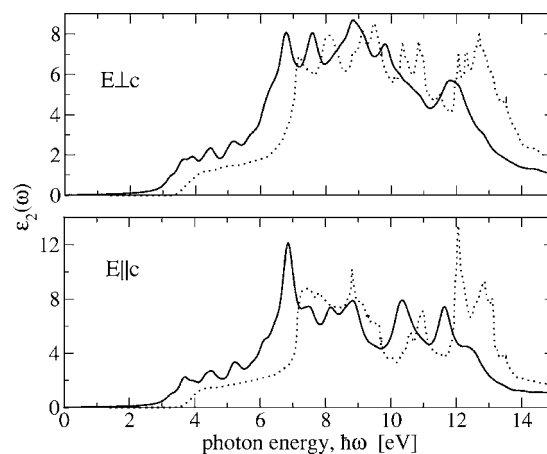


FIG. 1. Imaginary part of the dielectric function  $\varepsilon_2(\omega)$  calculated within the BSE formalism (full line) and the DFT with scissors shift one (dotted line) for two polarizations of the incoming light (perpendicular and parallel in the upper and lower panels, respectively). The polarization is given with respect to the  $c$  direction of the hexagonal unit cell. A broadening of 0.2 eV was used to generate the BSE curves. It should be noted that due to the relatively small number of  $\mathbf{k}$  points and the broadening the details around the gap edge are not reliable.

This is most striking for the case of parallelly polarized light ( $\mathbf{E} \parallel \mathbf{c}$ ), with the appearance of a dominant peak around 6.5 eV and the reduction of the peak around 12 eV in the BSE calculation.

#### B. Excitonic spectra and binding energies

The (two-particle) excitation energies of the system are given by the eigenvalues of the BSE Hamiltonian in Eq. (1). The levels lying inside the band gap are the most interesting as they correspond to bound excitons. In the usual interpretation based on Elliott’s model (hydrogenlike spectrum), the lowest state is considered to be the ground state of the exciton, whereas the higher levels are viewed as excited states of that exciton. For wurtzite GaN we have calculated three such ground states. As aforementioned, their spectral weights,  $A_{vck}^{\lambda}$ , are strongly localized around the  $\Gamma$  point of the BZ (as expected for a direct-gap semiconductor). Figure 2 shows schematically the gap-edge states<sup>41</sup> at  $\Gamma$ . Only the three highest valence (N- $p$  character) and the lowest conduction bands (Ga- and N- $s$  character) are found to be contributing to the excitonic wave functions. Two of these excitons ( $A, B$ ) are optically active (i.e., the oscillator strengths are nonzero) for light with  $\mathbf{E} \perp \mathbf{c}$ , and one ( $C$ ) for  $\mathbf{E} \parallel \mathbf{c}$ . Furthermore, anticipating the more detailed discussion of the excitonic wave functions below (see also Figs. 4 and 5), it turns out that the  $A$  and  $B$  excitons originate from the two upmost valence bands, whereas the  $C$  exciton comes from a hole in the next valence band below.

The calculated excitonic spectra, both for perpendicular and parallel polarizations of the incident light, are presented in Fig. 3. The experimental structural parameters, as well as a  $\mathbf{k}$ -point sampling covering a  $1/12 \times 1/12 \times 1/8$  part of the full BZ with a fine  $11 \times 11 \times 11$  mesh, were used for their

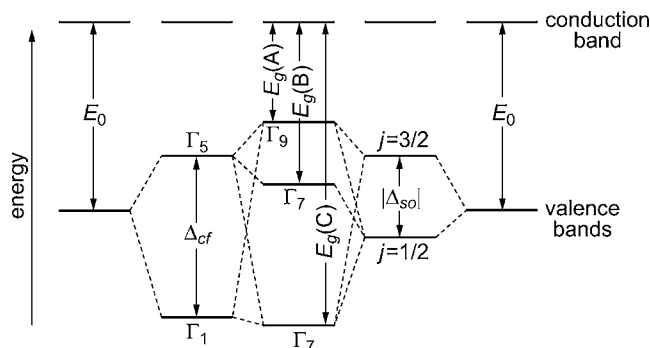


FIG. 2. Schematic energy-level diagram of band splitting under action of the crystal-field and spin-orbit interactions in wurtzite crystals (from Ref. 41). To the left, splitting induced only by the crystal field; to the right, splitting induced only by the spin-orbit interaction. The combined case is shown in the middle. The gaps  $E_g(A)$ ,  $E_g(B)$ , and  $E_g(C)$  which enter in the calculations of the binding energies of  $A$ ,  $B$ , and  $C$  excitons, respectively, are indicated in the middle. Note, however, that our basic BSE calculations did not include spin-orbit coupling (see discussion in text). In GaN our fully relativistic DFT calculations show that the final splitting of  $\Gamma_5 \rightarrow \Gamma_7, \Gamma_9$  is  $\approx 5$  meV.

evaluation. Note that the excitation energy scale for both polarizations has been shifted by the value of the optical band gap  $E_g = 3.45$  eV. On this scale, the lowest bound states are the  $A$  and  $B$  excitons (which are degenerate since we neglect SOC) at  $-37$  meV for  $\mathbf{E} \perp \mathbf{c}$  and the  $C$  exciton at  $-12$  meV for  $\mathbf{E} \parallel \mathbf{c}$ . Apart from a slight shift of the eigenenergies (due to the change in the dielectric function), the excitonic spectrum does not depend on the polarization. However, the polarization effects the oscillator strengths. This is exemplified by the presence of the zero weight lowest  $AB$  excitons in the  $\mathbf{E} \parallel \mathbf{c}$  panel of Fig. 3 as well as the second lowest  $C$  eigenstate in the  $\mathbf{E} \perp \mathbf{c}$  panel. The excitation energy

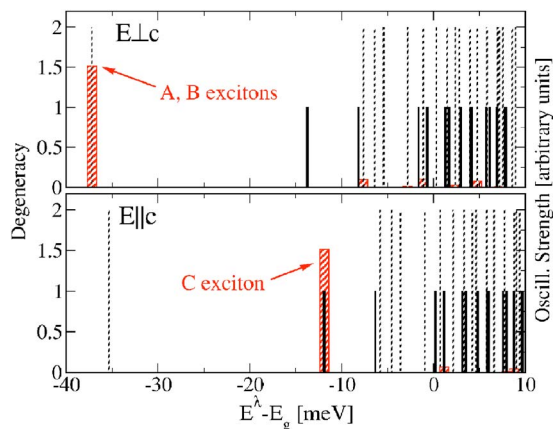


FIG. 3. (Color online) The calculated exciton spectra of GaN relative to the fundamental optical band gap  $E_g$  for light polarization perpendicular (top panel) and parallel (lower panel) to the crystallographic  $c$  direction. Both degeneracy and oscillator strength are shown. The dashed lines represent  $A$  and  $B$  excitonic levels (degenerate), solid lines represent  $C$  excitons, bars show the oscillator strength for corresponding levels. For  $\mathbf{E} \parallel \mathbf{c}$  the binding energy is not equal to  $E_g - E^\lambda$  (see text, and Fig. 2).

is the energy that should be given to the semiconducting ground state in order to create an interacting electron-hole pair. On the other hand, the exciton binding energy is the energy which is necessary to dissociate this pair. In other words, the excitation energy of a given exciton is the energy difference between the exciton level and the top of the originating valence band, whereas the corresponding binding energy is simply obtained by subtracting the calculated excitation energy from the noninteracting electron-hole pair energy. This noninteracting (or dissociated) electron-hole pair energy is the energy difference between the originating bottom conduction and top valence levels, namely, the *relevant* gaps  $E_g(A)$ ,  $E_g(B)$ , or  $E_g(C)$  in Fig. 2. Exciton binding energies are usually estimated from experiments through the application of Elliott's model.<sup>29</sup> This means that the binding energy is derived from the energy difference between two excitations which are supposed to belong to *one same* hydrogenlike spectrum. From our calculations, the binding energies of the three lowest excitons are 37 meV for  $A$ ,  $B$ , and 35 meV for  $C$  (still neglecting the spin-orbit effect, which in the present case is small). Note that a simple difference between the excitation energies and the optical band gap (i.e., 12 meV, see Fig. 3) does not give the correct binding energy for the  $C$  exciton because this difference does not take into account the crystal field splitting of 23 meV of the originating valence band. In agreement with experimental results, the calculated binding energies for the  $A$ ,  $B$ , and  $C$  excitons are close to each other. Our values are however about 10 meV too large when compared to experimental findings which lie in the range 18–28 meV. Although this discrepancy might seem large in relative terms, it is, in fact, very small when considering the approximations that have to be used in the construction of the BSE Hamiltonian (e.g., DFT wave functions, RPA for the screening of the Coulomb interaction). The RPA calculated  $\epsilon_{00}(q=0)$  are 5.2 for  $\mathbf{E} \perp \mathbf{c}$  and 5.3 for  $\mathbf{E} \parallel \mathbf{c}$ . These values are about 10% smaller than the  $\omega \rightarrow 0$  extrapolated values obtained from the experimental  $\epsilon(q=0, \omega)$ .<sup>5</sup> Assuming this underestimate applies uniformly to the whole dielectric matrix, it would explain our overestimate of the binding energies. Indeed, the binding energies are roughly proportional to  $\epsilon^{-2}$  since (i) the direct interaction term of the Hamiltonian [Eq. (4)] depends linearly on  $\epsilon^{-1}$  and (ii) the excitonic wave functions become more localized in  $k$  space with increasing  $\epsilon^{-1}$ . This is in fact in agreement with a simple hydrogen model. This results in a 20% (i.e., about 8 meV) overestimate of the calculated binding energies and would explain the discrepancy with experimental findings.

The definition of the binding energy used above can be easily applied only when the noninteracting  $e$ - $h$  pair at the origin of the exciton can be identified. Indeed, this may not be the case for strong  $e$ - $h$  interaction since the interacting  $e$ - $h$  pair wave function would then be a mixture of several noninteracting states. For such a strong  $e$ - $h$  interaction, it may be necessary to adiabatically switch it off in order to reveal the dissociated state corresponding to that exciton. This is, however, not necessary in practice as the  $e$ - $h$  interaction is generally much smaller than the diagonal part of the effective Hamiltonian in Eqs. (2)–(5) and only amounts to a relatively weak mixing the noninteracting dissociated states

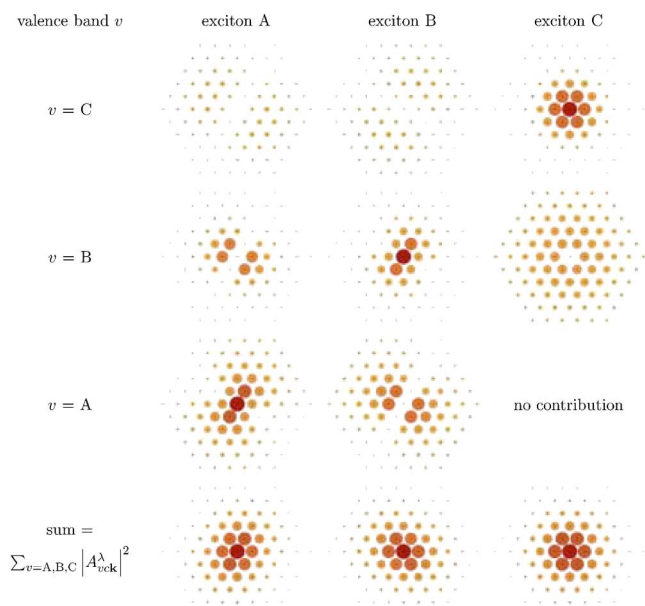


FIG. 4. (Color online) Absolute values of the weights  $A_{vc\mathbf{k}}^\lambda$ , defining the excitonic wave function plotted in the reciprocal space for the three highest valence and the lowest conduction band. The  $\mathbf{k}$  points lie in the basal plane of the hexagonal BZ and are shown as small black dots (the  $\Gamma$  point being at the center of each plot). The sampled  $k$  points span a fraction of  $1/12 \times 1/12$  of the BZ in this plane with a mesh of  $11 \times 11$  points. The absolute values of the expansion coefficients  $|A_{vc\mathbf{k}}^\lambda|$  are represented by the colors and sizes of the filled circles (the color map and diameters are, in fact, scaled as the square root of these absolute values in order to improve the visibility of small weights) and range from 0 (no circle) to about 0.22 (largest and darkest circles). The scale is kept constant for all figures.

(as is the case for GaN). This is most straightforward for the fully delocalized (in real space) part of the excitonic wave function (i.e., the part that is most “noninteractinglike”), the component at  $\Gamma$ , for which the corresponding noninteracting dissociated state can be easily identified (see Fig. 4).

The  $\mathbf{k}$ -space dispersion of the excitonic wave function is important for practical calculations of the binding energies. It is, therefore, interesting to see which bands and  $\mathbf{k}$  points contribute to the different excitons. This is shown in Fig. 4 where the absolute values of the weights  $A_{vc\mathbf{k}}^\lambda$  are plotted for  $\mathbf{k}$  points in the (001) plane passing through the  $\Gamma$  point. The colormap and the circle diameters are scaled proportionally to the square root of  $|A_{vc\mathbf{k}}^\lambda|$  in order to improve the visibility of small values (this scale is kept constant throughout Fig. 4). The different contributing valence bands are (conveniently) labeled by the  $v=A, B, C$  index. Valence band C is mainly of  $p_z$  character at  $\Gamma$ , whereas the bands A and B are of mixed  $p_x$  and  $p_y$  character (and are degenerate in the absence of SOC). The A exciton is clearly dominated by contributions from band  $v=A$ , but contributions from band B are quite important outside the  $\Gamma$  point. The opposite is true for the B exciton. Exciton C is mainly of valence band C character, with some weight on band B outside the  $\Gamma$  point. Contrary to the C exciton, the A and B ones seem not to satisfy hexagonal symmetry requirements (apparent absence of six-

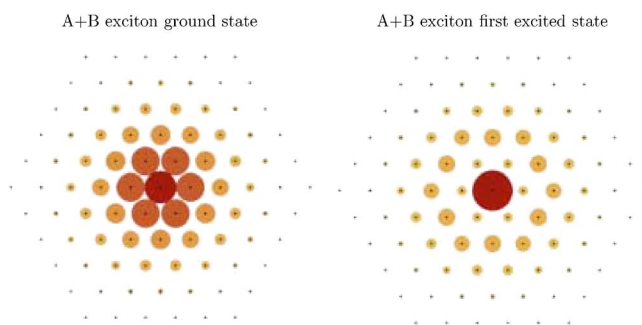


FIG. 5. (Color online) Excitonic wave function weights for the sum of the A and B excitons in the ground and the first excited states. The same representation and scale as for Fig. 4 is used (except that the maximum value of the weights is about 0.25 here).

fold symmetry). This is because they are degenerate and, as shown in Fig. 5, their sum displays the hexagonal symmetry as it should be. This figure shows in addition that the first excited state is much more localized in  $\mathbf{k}$  space than the ground state (more delocalized in the real space), which is expected since the excited state lying closer to the conduction band, it should have more similarities with the noninteracting or dissociated state.

Figure 6 shows the binding energies plotted as a function of the change in the unit cell volume. Since only the ground states of the three excitons are considered here, the computing time can be considerably reduced by using the less dense sampling (equivalent to nearly  $5 \times 10^5$ , see Sec. II). We assume that our GGA single-particle calculations correctly reproduce the change of the band gap, and we therefore use a constant value of the scissor shift (1.4 eV). For small and intermediate compressions (up to 4% volume change), there is a small but visible increase of the binding energies with pressure. Larger compressions result in a fast decrease of the binding energies which is due to an enhanced screening of the Coulomb  $e$ - $h$  interaction caused by an increase of the

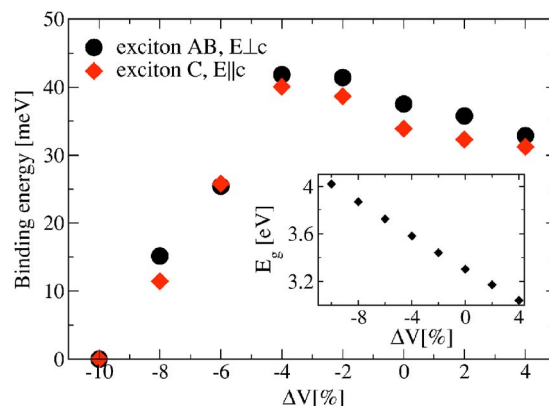


FIG. 6. (Color online) Binding energies for the ground state of bound excitons as a function of the relative change of the unit cell volume with respect to the experimental one (for constant  $c/a$  and  $u$ ). These are shown for excitons A and B with perpendicularly polarized light (circles) and exciton C with parallelly polarized light (diamonds). The inset shows the volume dependence of the optical gap  $E_g$ .  $\Delta V=0$  corresponds to the experimental equilibrium volume.

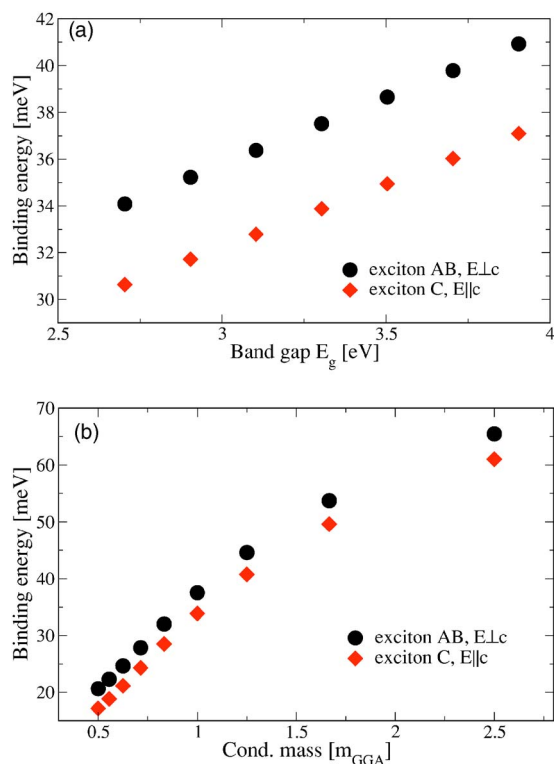


FIG. 7. (Color online) Dependence of the bound exciton binding energies on (a) the band gap, and (b) the conduction band mass, plotted for excitons  $A$ ,  $B$  ( $\mathbf{E} \perp \mathbf{c}$ ), and  $C$  ( $\mathbf{E} \parallel \mathbf{c}$ ). The band gap was varied by simply rigidly shifting the conduction band and the conduction band mass by rescaling the bandwidth. The calculations were done for the experimental structural parameters.

overlap between atomic Ga and N states. A similar behavior has been observed recently in organic semiconductors.<sup>37</sup> The slow increase for low compressions is related to the increase of the band gap when the unit cell is compressed. The inset of Fig. 6 displays the corresponding volume dependence of the optical band gap  $E_g$ . Figure 7(a) shows that the binding energies depend linearly on the gap, a 0.5 eV change of which resulting in a change of the binding energies of about 4 meV (the gap was changed by simply varying the scissors shift  $\Delta$ ). This can be simply understood from Eqs. (2)–(5). According to the Penn model<sup>42</sup> the dielectric constant can be simply approximated by  $\epsilon(0) = 1 + (\hbar\omega_p/E_g)^2$ . In the considered range of  $E_g$ , it is nearly inversely proportional to the gap and the screened interaction in Eq. (4) is therefore roughly proportional to  $E_g$ . As a result, the binding energy increases with it [note that the large diagonal part in Eq. (3) is, in fact, subtracted from the Hamiltonian when determining the binding energies]. Therefore, the increase of the binding energies with pressure for low compression rates, for which the overlap of the wave functions can be considered as constant, is a direct effect of the change of the gap. Such an increase has indeed been observed experimentally<sup>25</sup> for pressures in the range 0–6 GPa (i.e., up to about 2% volume change).

As already stated in Sec. II, quasiparticle states should, in principle, be used as a basis for exciton wave functions in the formulation of the BSE Hamiltonian. Nevertheless, we employ here the DFT-GGA single-particle states (the DFT wave

functions being good approximations to quasiparticle ones<sup>32</sup>) and correct the well-known “band gap problem” through a simple rigid shift  $\Delta$  of the conduction band. However, the bandwidths of conduction bands are known to be overestimated by DFT (GGA or LDA) with respect to  $GW$ , and we have performed calculations in which the mass of the conduction band was artificially varied in order to see the effect on the binding energies. This is shown on Fig. 7(b). The wave functions were not changed and the mass was varied by simply scaling the bandwidth of the conduction band. For reference, the calculated band mass for the experimental lattice constant is  $0.175m_0$ , which is close to the reported experimental value of  $0.2m_0$  at 300 K.<sup>43</sup> The binding energies are found to be increasing monotonically with increasing conduction band mass and to be only moderately affected by it, changing by about 10% for a 5% variation of the mass. This increase is consistent with the two limiting cases of very small masses (very large bandwidths) for which the interaction is almost fully screened resulting in a zero binding energy and of very large masses (flat bands) for which the screening is smaller and the binding energy maximum.

Most of the experiments on GaN are done using epitaxially grown samples. Depending on the substrate, some strains can be induced in the sample, and to see how their effect on the binding energies, we have performed a series of calculations for different deformations of the unit cell (at constant volume). The binding energies were essentially unaffected by varying  $c/a$  (within  $\pm 2\%$ ) and  $u$  (from 0.369 to 0.385). On the other hand, the excitation energies were found to change significantly, because the positions of the valence bands depend strongly on  $u$ .

Spin-orbit coupling effects were neglected in all the calculations presented above. Their inclusion would increase the size of the BSE Hamiltonian by a factor of 4.<sup>44</sup> In the case of GaN, this simplification is acceptable in our opinion. Indeed, our relativistic DFT calculations have shown that the SOC induced splitting of the valence N- $(p_{x,y})$  bands (i.e.,  $\Gamma_5 \rightarrow \Gamma_7, \Gamma_9$  in Fig. 2) is only of the order of 5 meV, which is much smaller than the typical excitonic binding energy of 35 meV. Furthermore, although the excitation energies will be shifted by a value approximately equal to this splitting, the effect on the binding energies is expected to be much smaller. This follows from the relative insensitivity of the binding energies to changing the band gap, as demonstrated by Fig. 7(a) (note that, on the contrary, the excitation energies tend to follow directly changes in the band gap). Apart from lifting the degeneracy, the SOC also affects the oscillator strengths: With SOC the  $B$  and  $C$  valence states have the same symmetry (i.e.,  $\Gamma_7$ ; see Fig. 2 and Ref. 41), and their character is now a mixture of  $p_x, p_y$ , and  $p_z$ . As a consequence, in opposition to the non-SOC case, both  $B$  and  $C$  excitons can now be excited for *any* polarization of the incident light (i.e., for  $\mathbf{E} \perp \mathbf{c}$  as well as for  $\mathbf{E} \parallel \mathbf{c}$ ). It must be noted, however, that, because of the small effect of the SOC on the bands and their characters (only about 2% mixing), the oscillator strengths for the  $B$  and  $C$  excitons, for  $\mathbf{E} \parallel \mathbf{c}$  and  $\mathbf{E} \perp \mathbf{c}$ , respectively, although nonzero, will remain extremely small. This means that, for practical considerations, our results would be left essentially unchanged by the inclusion of SOC.

The large number of excitonic levels as well as the variety of their behaviors with respect to polarization of the light make the detailed analysis and the interpretation of experimental data very difficult. Even in the absence of SOC effects, we are left with three different excitonic ground states. Apart from lifting the degeneracy of the  $A, B$  excitons, including SOC implies that the number of excitonic ground states can be further increased because of the exchange term in the BSE Hamiltonian. For the case of GaN, the main difficulty in correctly interpreting experimental spectra comes from the fact that the crystal field splitting [which is responsible for the 25 meV difference between the excitation energies of the ( $A, B$ ) and  $C$  excitons] is close to the energy difference between the ground and first excited state of the  $A, B$  excitons. Therefore, in a nonpolarized experiment, exciton  $C$  could be misinterpreted as the first excited state of exciton  $B$ , leading to an incorrect estimate of the binding energies. This could be the case for the lowest of these experimental estimates (i.e., 18 meV) as suggested in Ref. 27, particularly because of the large sensitivity of the crystal field splitting on the shape of the unit cell and the fact that epitaxially layered samples were used in those experiments.

#### IV. SUMMARY AND CONCLUSION

In this paper, we have presented *ab initio* calculations of the optical response of wurtzite GaN. The electron-hole interaction was accounted for by solving the Bethe-Salpeter equation. The calculated imaginary part of the dielectric function for frequencies above the fundamental band gap was found to be in good agreement with previous theoretical and experimental results. For this, since we were primarily interested in relatively broad features of the spectrum, we could use a “time-evolution” algorithm, in which neither the excitonic wave functions nor the excitation energies were explicitly calculated, in order to reduce the computational difficulties caused by the large size of the BSE Hamiltonian. The calculation of excitation energies *inside* the band gap (bound excitonic states) is, however, more delicate and required a computationally intensive direct diagonalization of the Hamiltonian. Moreover, as the excitonic wave functions turned out to be very localized around the  $\Gamma$  point, only a small fraction of the Brillouin zone around this point had to be sampled, but an extremely dense  $\mathbf{k}$  point mesh had to be used. Spin-orbit coupling was neglected in all our BSE calculations, but fully relativistic electronic structure calcula-

tions have shown that its effect at the valence band maximum is particularly small in wurtzite GaN (about 5 meV). The lowest excitations have been associated with the ground states of three bound excitons, labeled  $A$ ,  $B$ , and  $C$ . The  $A, B$  excitons are degenerate when spin-orbit coupling is neglected and are mainly composed of Ga-/N- $s$  and N-( $p_{x,y}$ ) states. The  $C$  exciton originates mainly from Ga-/N- $s$  and N- $p_z$  states. In the absence of spin-orbit coupling, the oscillator strengths of the  $A, B$  excitons are nonzero only for perpendicularly polarized light, whereas the  $C$  exciton is active only for parallelly polarized light (with respect to the  $c$  direction). The excitonic binding energy is defined as a difference between the separation of the (quasiparticle) conduction and valence bands contributing to that exciton and the excitation energy. For the experimental unit cell parameters, the calculated binding energies of the degenerate  $A, B$  excitons are 37 meV and 35 meV for exciton  $C$ . These were found to be mostly insensitive to changing the shape of the unit cell ( $c/a$  ratio and Ga–N distance in the  $c$  direction,  $u$ ) and to be slightly increasing with increasing pressure for volume changes of up to 4% in agreement with experimental findings. We estimate that the inclusion of spin-orbit coupling in the BSE Hamiltonian would result in splitting the  $A, B$  excitons binding energies by only a few meV and would, therefore, not affect our main conclusions. Nevertheless, SOC affects the symmetry of the valence states so that both the  $B$  and  $C$  excitons become active (nonzero oscillator strengths) for both polarizations. This and the fact that the crystal field splitting is of the same order of magnitude as the excitonic binding energies make the interpretation of experimental results particularly delicate.

#### ACKNOWLEDGMENTS

We are grateful to the “EXCITING” and “ $f$ -electron” European Research and Training Networks for providing financial support (Contract Nos. HPRN-CT-2002-00317 and HPRN-CT-2002-00295, respectively). C.A.D. appreciates support from the Austrian Science Fund, Project No. P16227. N.E.C. acknowledges support from the Danish Natural Science Research Council, Grant No. 21-03-0340. The calculations were performed at the Center for Scientific Computing in Aarhus (CSCAA), financed by the Danish Center for Scientific Computing (DCSC) and the Faculty of Science, University of Aarhus. We are grateful to N.C. Hansen, system manager at CSCAA, for excellent advice in connection with our heavy computing tasks.

<sup>1</sup>S. Nakamura, M. Senoh, N. Iwasa, and S. Nagahama, *Appl. Phys. Lett.* **67**, 1868 (1995).

<sup>2</sup>S. Nakamura, M. Senoh, S. Nagahama, N. Iwasa, T. Yamada, Y. Sugimoto, and H. Hiyoku, *Appl. Phys. Lett.* **70**, 1417 (1997).

<sup>3</sup>B. W. Lim, Q. C. Chen, J. Y. Yang, and M. A. Khan, *Appl. Phys. Lett.* **68**, 3761 (1996).

<sup>4</sup>S. Nakamura, *The Blue Laser Diode-GaN based Light Emitters*

*and Lasers* (Springer, Berlin, 1997).

<sup>5</sup>P. Perlin, I. Gorczyca, N. E. Christensen, I. Grzegory, H. Teisseyre, and T. Suski, *Phys. Rev. B* **45**, 13307 (1992).

<sup>6</sup>N. E. Christensen and I. Gorczyca, *Phys. Rev. B* **50**, 4397 (1994).

<sup>7</sup>K. Karch, J.-M. Wagner, and F. Bechstedt, *Phys. Rev. B* **57**, 7043 (1998).

<sup>8</sup>L. X. Benedict and E. L. Shirley, *Phys. Rev. B* **59**, 5441 (1999).

- <sup>9</sup>L. X. Benedict, T. Wethkamp, K. Wilmers, C. Cobet, N. Esser, L. Shirley, W. Richter, and M. Cardona, *Solid State Commun.* **112**, 129 (1999).
- <sup>10</sup>S. Albrecht, L. Reining, R. Del Sole, and G. Onida, *Phys. Rev. Lett.* **80**, 4510 (1998).
- <sup>11</sup>L. X. Benedict, E. L. Shirley, and R. B. Bohn, *Phys. Rev. Lett.* **80**, 4514 (1998).
- <sup>12</sup>M. Rohlfing and S. G. Louie, *Phys. Rev. Lett.* **81**, 2312 (1998).
- <sup>13</sup>L. J. Sham and T. M. Rice, *Phys. Rev.* **144**, 708 (1966).
- <sup>14</sup>W. Hanke and L. J. Sham, *Phys. Rev. B* **12**, 4501 (1975).
- <sup>15</sup>W. Hanke and L. J. Sham, *Phys. Rev. Lett.* **43**, 387 (1979).
- <sup>16</sup>W. Hanke and L. J. Sham, *Phys. Rev. B* **21**, 4656 (1980).
- <sup>17</sup>G. Strinati, *Phys. Rev. Lett.* **49**, 1519 (1982).
- <sup>18</sup>G. Strinati, *Phys. Rev. B* **29**, 5718 (1984).
- <sup>19</sup>S. Albrecht, G. Onida, and L. Reining, *Phys. Rev. B* **55**, 10278 (1997).
- <sup>20</sup>M. Rohlfing and S. G. Louie, *Phys. Rev. Lett.* **82**, 1959 (1999).
- <sup>21</sup>P. Puschnig and C. Ambrosch-Draxl, *Phys. Rev. Lett.* **89**, 056405 (2002).
- <sup>22</sup>D. G. Chitchevina, Z. C. Feng, S. J. Chua, and G. D. Gilliland, *Phys. Rev. B* **63**, 125211 (2001).
- <sup>23</sup>A. K. Viswanath, J. I. Lee, D. Kim, C. R. Lee, and J. Y. Leem, *Phys. Rev. B* **58**, 16333 (1998).
- <sup>24</sup>G. D. Chen, M. Smith, J. Y. Lin, H. X. Jing, S.-H. Wei, M. Asif Khan, and C. J. Sun, *Appl. Phys. Lett.* **68**, 2784 (1996).
- <sup>25</sup>Z. X. Liu, S. Pau, K. Syassen, J. Kuhl, W. Kim, H. Morkoç, M. A. Khan, and C. J. Sun, *Phys. Rev. B* **58**, 6696 (1998).
- <sup>26</sup>S. J. Xu, W. Lui, and M. F. Li, *Appl. Phys. Lett.* **81**, 2959 (2002).
- <sup>27</sup>M. Steube, K. Reimann, D. Fröhlich, and S. J. Clarke, *Appl. Phys. Lett.* **71**, 948 (1997).
- <sup>28</sup>J. F. Muth, J. H. Lee, I. K. Shmagin, R. M. Kolbas, H. C. Casey, B. P. Keller, U. K. Mishra, and S. P. Den Baars, *Appl. Phys. Lett.* **71**, 2572 (1997).
- <sup>29</sup>R. J. Elliott, *Phys. Rev.* **108**, 1384 (1957).
- <sup>30</sup>M. Corti, A. Gabetta, M. Fanciulli, A. Svane, and N. E. Christensen, *Phys. Rev. B* **67**, 064416 (2003).
- <sup>31</sup>L. Hedin and S. Lundqvist, *Solid State Phys.* **23**, 1 (1969).
- <sup>32</sup>M. S. Hybertsen and S. G. Louie, *Phys. Rev. B* **34**, 5390 (1986).
- <sup>33</sup>S. L. Adler, *Phys. Rev.* **126**, 413 (1962).
- <sup>34</sup>N. Wiser, *Phys. Rev.* **129**, 62 (1963).
- <sup>35</sup>P. Blaha, K. Schwarz, G. K. H. Madsen, D. Kvasnicka, and J. Luitz, *WIEN2K, An Augmented Plane Wave Plus Local Orbitals Program for Calculating Crystal Properties*. ISBN 3-9501031-1-2 (Vienna University of Technology, Austria 2001).
- <sup>36</sup>G. K. H. Madsen, P. Blaha, K. Schwarz, E. Sjöstedt, and L. Nordström, *Phys. Rev. B* **64**, 195134 (2001).
- <sup>37</sup>K. Hummer, P. Puschnig, and C. Ambrosch-Draxl, *Phys. Rev. Lett.* **92**, 147402 (2004).
- <sup>38</sup>P. Puschnig and C. Ambrosch-Draxl, *Phys. Rev. B* **66**, 165105 (2002).
- <sup>39</sup>J. P. Perdew, K. Burke, and M. Ernzerhof, *Phys. Rev. Lett.* **77**, 3865 (1996).
- <sup>40</sup>W. G. Schmidt, S. Glutsch, P. H. Hahn, and F. Bechstedt, *Phys. Rev. B* **67**, 085307 (2003).
- <sup>41</sup>L. C. Lew Yan Voon, M. Willatzen, M. Cardona, and N. E. Christensen, *Phys. Rev. B* **53**, 10703 (1996).
- <sup>42</sup>D. Penn, *Phys. Rev.* **128**, 2093 (1962).
- <sup>43</sup>V. Bangrov, M. E. Levinshtein, S. L. Rumyantsev, and A. Zubrilov, *Properties of Advanced Semiconductor Materials GaN, AlN, InN, BN, SiC, SiGe* (John Wiley & Sons Inc., NY, 2001).
- <sup>44</sup>M. Rohlfing and S. G. Louie, *Phys. Rev. B* **62**, 4927 (2000).